ORIGINAL PAPER

Dynamic sub-surface characteristic and the active faults of the Genç District locating over the Bingöl Seismic Gap of the East Anatolian Fault Zone, Eastern Turkey

Kenan Akbayram[1,2] · Erdem Bayrak[3,4] · Eren Pamuk[5] · Çağlar Özer[3,4] · Kemal Kıranşan[1,6] · Sadık Varolgüneş[1,2]

Abstract

The Genç District is located on the Bingöl Seismic Gap (BSG) of the Eastern Anatolian Fault Zone (EAFZ) with its ~ 34.000 residents. The Karlıova Triple Junction, where the EAFZ, the North Anatolian Fault Zone, and the Varto Fault Zone meet, is only 80 km NE of the Genç District. To make an earthquake disaster damage prediction of the Genç District, carrying a high risk of disaster, we have (1) prepared a new geological map, and (2) conducted a single-station microtremor survey. We defined that three SW-NE trending active faults of the sinistral Genç Fault Zone are cutting through the District. We have obtained dominant period (T) as < 0.2 s, the amplification factor (A) between 8 and 10, the average shear wave velocity for the first 30 m (Vs_{30}) as < 300 m/s, and the seismic vulnerability index (Kg) as > 20, in the central part of the Genç District. We have also prepared damage prediction maps for three bedrock acceleration values (0.25, 0.50, 0.75 g). Our earthquake damage prediction scenarios evidenced that as the bedrock acceleration values increase, the area of soil plastic behavior expands linearly. Here we report that if the average expected peak ground acceleration value (0.55–0.625 g) is exceeded during an earthquake, significant damage would be inevitable for the central part of the Genç District where most of the schools, mosques, public buildings, and hospitals are settled-down.

Keywords Bingöl Seismic Gap · Earthquake damage prediction · East Anatolian Fault Zone · Genç Fault Zone · Microtremor survey · Soil dynamic features

✉ Kenan Akbayram
  kakbayram@bingol.edu.tr

1 Centre for Energy, Environment and Natural Disasters, Bingöl University, 12000 Bingöl, Turkey

2 Department of Civil Engineering, Bingöl University, 12000 Bingöl, Turkey

3 Earthquake Research Centre, Ataturk University, 25240 Erzurum, Turkey

4 Department of Civil Engineering, Ataturk University, 25240 Erzurum, Turkey

5 Department of Geophysical Research, General Directorate of the Mineral Research and Exploration (MTA), 06800 Ankara, Turkey

6 Department of Geography, Bingöl University, 12000 Bingöl, Turkey

Fig. 1 **a** Active tectonic map of the Eastern Mediterranean and the Middle East. Thick lines indicate plate ▶ boundary fault zones. Thin black lines are faults formed in the Anatolian Plate, the dotted lines represent the position of the hanging wall of normal faults. White arrows and numbers indicate the global positioning system (GPS)–derived velocities (mm year^{-1}) with respect to Eurasia (Reilinger and McClusky 2011; Ergintav et al. 2014). **b** The fault map of the eastern sector of the Anatolian Plate and surrounding area, between Pülümür (Tunceli), Varto (Muş), Kulp (Diyarbakır) and Palu (Elazığ). For the location, see (**a**). The faults and their names are generally from Emre et al. (2013). Some faults are (e.g. Kığı Yayladere Fault Zone) drawn by us. The purple line in the upper corner, with 1939 over it, represents the southeastern part of the rupture of the M_w 7.9, 1939 Erzincan earthquake (Kalafat et al. 2009). The epicenter of this event is outside (**b**). Other purple faults are the ruptured fault segments during $6.4 \leq M \leq 6.9$ events in the last century. The numbers next to the epicenters are also given in Table 1, which contains the information of these earthquakes. The epicenter locations are from IRIS (2021) except the earthquake 7 which is defined by us (in preparation). For detailed earthquake data of $5.3 \leq M$ events, see Table 1. ASF: Afyon-Simav Fault; BZATZ: Bitlis Zagros Active Thrust Zone; DSFZ: Dead Sea Fault Zone; EFZ: Eskişehir Fault Zone; EAFZ: East Anatolian Fault Zone; EcFZ: Ecemiş Fault Zone; K: Karlıova, Karg. F.: Kargapazarı Fault; KTJ: Karlıova Triple Junction; NAFZ: North Anatolian Fault Zone; RAE: Region of Aegean Extension; SF: Sudüğünü Fault; SFZ: Sungurlu Fault Zone; SUFZ: Sancak Uzunpınar Fault Zone; TFZ: Tuz Gölü Fault Zone; VFZ: Varto Fault Zone

1 Introduction

It is impossible to prevent earthquakes, however, management of their effects and reducing loss of life, injuries, and structural damage is possible (Nakamura 1996; Adnan et al. 2015). Earthquake disaster management starts with migitation that includes seismic zoning, and vulnerability (or damage prediction) analyses (Nakamura 1996; Adnan et al. 2015). In this study, we present the results of the first multi-disciplinary seismic vulnerability analyses of the Genç District (City of Bingöl, E Turkey) as the first step of earthquake disaster management. The Genç District is located at the southern border of the Bingöl Pull-Apart Basin that formed along the East Anatolian Fault Zone (EAFZ). The ~430-km-long, left-lateral strike-slip EAFZ is the active plate boundary between the Anatolian and Arabian lithospheric plates (Fig. 1a) (Şengör 1979; Reilinger and McClusky 2011; Ergintav et al. 2014). The EAFZ and the ~1400-km-long dextral North Anatolian Fault Zone (NAFZ) together accommodate the westward escape of the Anatolian plate (Fig. 1a) (McKenzie 1972; Şengör 1979; Cavalié and Jónsson 2014). The EAFZ connects with the NAFZ and Varto Fault Zone (VFZ) at the Karlıova Triple Junction (KTJ), ~80 km NE of the Genç District (Fig. 1a, b) (Şengör 1979; Şaroğlu 1985; Şengör et al. 1985; Hubert-Ferrari et al. 2002; Seyitoğlu et al. 2019). The segments of the EAFZ near and around the Genç District are parts of the Bingöl Seismic Gap (Fig. 1b) (Nalbant et al. 2002; Duman and Emre 2013; Akbayram et al. 2021). The Yedisu Seismic Gap of the NAFZ (Fig. 1b), capable of creating a 7.2 M_w earthquake (Zabcı et al. 2017), is only 90 km NE of Genç District. In addition to these two major seismic gaps, there are other active faults capable of 6.3 M_w earthquakes (Fig. 1b; Table 1) both at the north (e.g., Sudüğünü Fault and Nazımiye-Karakoçan-Bingöl Fault Zone) and at the south of the Genç District (e.g., Yayla and Yenisu Faults). Hence, the Genç District having ~34.000 residents, important iron-ore enterprises, major railroads, and highways, is not only surrounded by but also staying over the seismic hazard sources.

To make an earthquake disaster damage prediction of the Genç District, we have held geological and geophysical surveys in and around the main residential area of the Genç District. During our geological survey, we defined the active faults cutting through the Genç District that are the nearest seismic hazard sources. We have also examined some previously collected geotechnical well-logs to understand the changes throughout the soil stratigraphy. As a crucial part of earthquake disaster damage prediction, we conducted a
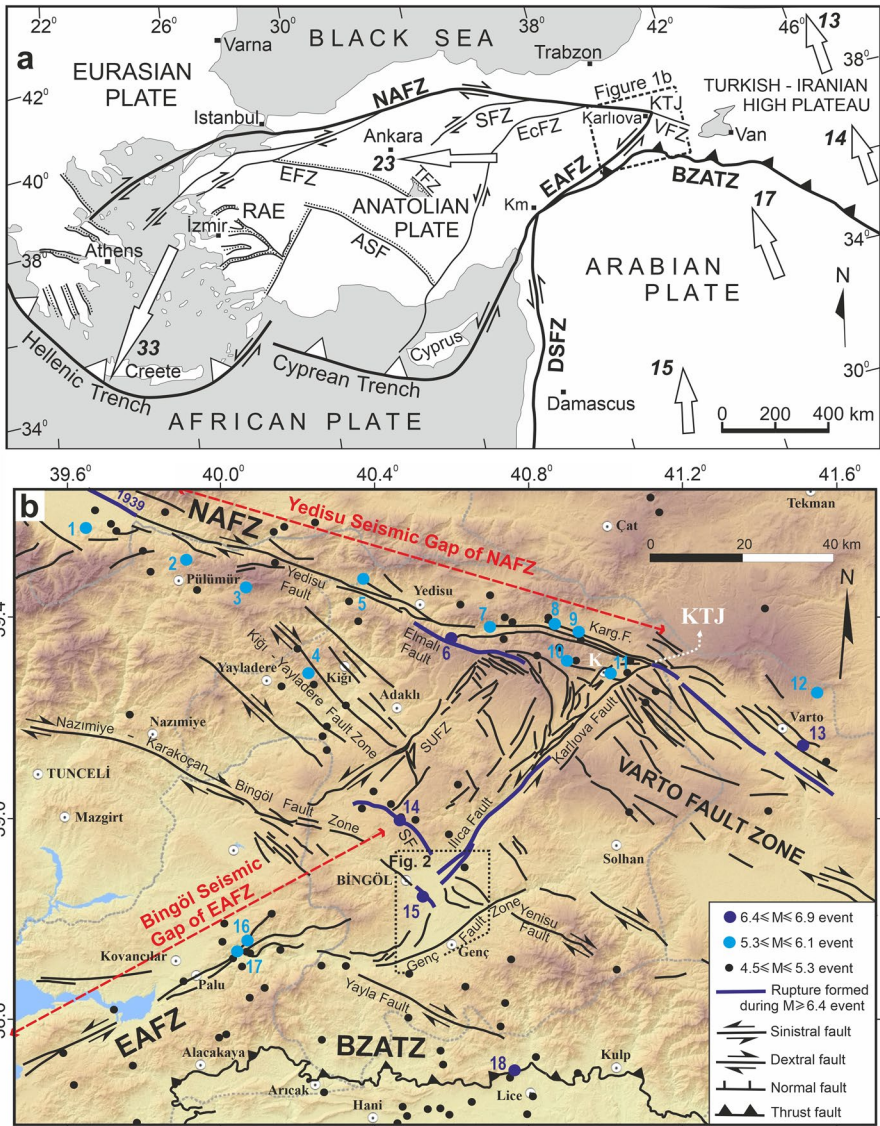
single station microtremor survey covering a ~ 9 km² area for understanding the dynamic behavior of the Quaternary soil that the Genç District established over. As a result of our analyses, we have prepared the following maps of the Genç District; (1) structural-stratigraphic geological map, (2) the average dominant period (*T*) map, (3) the soil amplification factor (*A*) map, (4) the bedrock depth map, (5) the seismic vulnerability index (*Kg*) map, and (6) the shear wave velocity (*Vs₃₀*) map. The average dominant period (*T*) of soils is an important parameter used in earthquake-soil-structure interaction studies (Vucetic 1992; Stanko et al. 2017). Obtaining this parameter is essential to take the necessary measures before an earthquake for damage reduction (Lomnitz 1999). In some cases, soil layers

Table 1 The seismic and damage data of $M \geq 5.3$ earthquakes occurred along the area shown in the Fig. 1b

Eventno Fig. 1b	Mag	Date (dd/mm/yy)	Time (hh:mm)[a]	Epicenter Lat (N°)		Maximum intensity[b]	Number of kills	Damaged buildings	References
1	6.1	27/01/2003	05:26	39.58	39.66	VII	1	50	1,2
2	5.8	15/03/1992	16:16	39.53	39.93	VII	–	439	2,3
3	5.7	05/12/1995	18:49	39.43	40.11	VI+	1	–	2,3
4	5.3	02/12/2015	01:27	39.29	40.23	?	?	?	4
5	5.9	26/07/1967	18:53	39.50	40.40	VIII	97	1282	5,6,7
6	6.9	17/08/1949	18:44	39.39	40.61	IX	450	3500	2,8,9
7	5.9	14/06/2020	14:24	39.37	40.74	VII	1	800	10
8	5.4	23/03/2005	23:44	39.41	40.80	VI	–	–	2,11
9	5.6	12/03/2005	07:36	39.41	40.86	VI	–	–	2,11
10	5.9	14/03/2005	01:55	39.41	40.81	VII	–	3349[c]	2,11
11	5.7	06/06/2005	08:41	39.38	40.84	VI	–	?	2
12	5.6	07/03/1966	01:16	39.20	41.60	VIII	14	1100	2,3
13	6.9	19/08/1966	12:22	39.17	41.56	IX	2396	20,007	2,3
14	6.4	01/05/2003	00:27	39.04	40.53	VIII	176	6000	1,2
15	6.8	22/05/1971	18:43	38.83	40.52	VIII	878	9111	2,12
16	6.1	08/03/2010	04:32	38.76	40.08	VII	42[d]	>4000[d]	2,13
17	5.6	08/03/2010	07:47	38.70	40.05	VI	–	–	14
18	6.0	06/09/1975	09:20	38.51	40.77	VIII	2385	8149	2,3
19[e]	7.9	26/12/1939	01:57	39.80	39.51	X–XI	32,968	116,720	1,2

References: 1: Kalafat et al. (2009); 2: KOERI (2021); 3:Tan et al. (2008); 4: Altuncu Poyraz et al. (2019); 5: Eyidogan et al. (1991); 6: McKenzie (1972); 7: AFAD (2021); 8: Ambraseys and Jackson (1998); 9: Nalbant et al. (2002); 10: Akbayram et al. (2021); 11: Demirtaş (2019); 12: Taymaz et al. (1991); 13: Tan et al. (2011); 14: USGS (2021)

[a]UTC time

[b]Modified Mercalli Scale

[c]Total number of three following events (12, 14, and 23 March 2005)

[d]Total number of two following events (04:32, and 07:47/8 March 2010)

[e]Epicenter of this event is outside the Fig. 1b, however part of it's rupture reaches to the map (see Fig. 1b)

cause an increase in the amplitude of earthquake waves at some frequencies, as a result, soil amplification (*A*) occurs, and the amplitude of earthquake waves passing from compact bedrock to soft soil layers increases (Kawase 2003; Mucciarelli et al. 2004; Yalçınkaya 2010). Bedrock depth and its geometry are particularly important in geotechnical studies that can be considered as the depth at which earthquake waves will significantly change their frequency content (Yalçınkaya 2010; İyisan and Haşal 2011). Shear wave velocity (*Vs*), one of the most important parameters used to determine the dynamic behavior of the soil during an earthquake, is widely used in the calculation of soil dynamic parameters and liquefaction analysis (Tokimatsu and Uchida 1990; Andrus and Stokoe 2000; Youn et al. 2008; Kayen et al. 2013; L'Heureux and Long 2017). According to Nakamura (1997), earthquake-related structural damage and the seismic vulnerability index values (*Kg*) are associated with the dominant frequency (*T*) and amplification factor (*A*) values that are related to each other. The structural damage of an earthquake increases if the *Kg* value is greater than 20, hence, *Kg* can be used to estimate possible structural damage that may occur during an earthquake (Nakamura 1997, 2019). Using determined *A, T, Kg*, and *BD*, we have calculated the shear strain distribution for three bedrock acceleration values (0.25, 0.50, and 0.75 g), and prepared the possible earthquake damage prediction maps for each value for the Genç District.

2 Major seismic sources and the regional geology

The NAFZ, the EAFZ, the VFZ, and the Bitlis-Zagros Active Thrust Zone (BZATZ) (Fig. 1a) are the products of the neotectonic period started with the collision of the Anatolian Block and the Arabian Plate in Anatolia (Şengör 1980). The intense earthquake activity around the KTJ has been revealed by historical earthquake records and instrumental measurements of earthquake activities (Fig. 1b; Table 1) (McKenzie 1972; Seymen and Aydın 1972; Arpat and Şaroğlu 1972; Ambraseys 1989; Taymaz et al. 1991; Ambraseys and Jackson 1998; Herece 2008; Tan et al. 2008; Emre et al. 2013; Duman and Emre 2013; Seyitoğlu et al. 2019). In this section, first, we introduce (1) the major seismic sources that may create earthquakes causing possible damage in the Genç District and then (2) the geological units cropping out in and around the Bingöl Pull-Apart Basin to make our new geological map cognizable for the reader's who are not familiar with the geology of the region.

2.1 Yedisu Seismic Gap of the NAFZ

The studies held after the destructive 7.9 M_w 1939 Erzincan earthquake (Fig. 1b; Table 1) (e.g., Allen 1969; Ambraseys 1970; Andrieux et al. 1995; Ataman et al. 1975; Barka 1992; Dewey and Şengör 1979; Ketin 1948, 1957, 1969; Pavoni 1962; Şengör et al. 2005; Şengör and Canitez 1982) proved that approximately 1100 km of the 1400-km-long NAFZ have been ruptured in the last century (cf., Şengör et al. 2005). The last major seismic event that occurred along the eastern part of the NAFZ is the 6.9 M_s, 17 August 1949 earthquake formed a 38-km-long rupture along the Elmalı Fault (Fig. 1b; Table 1) (Ambraseys and Jackson 1998; Nalbant et al. 2002). The maximum intensity of the 1949 earthquake had reached IX (Table 1) (Ambraseys 1989; Ambraseys and Jackson 1998). However, on the Yedisu Fault which is between the rupture zone of the 1939 and 1949 events (Fig. 1b), the last destructive earthquake occurred in 1784 (Barka et al. 1987). Calculations show that the Yedisu Fault is capable of a 7.2 M_w earthquake with possible meters of co-seismic

rupture (Zabcı et al. 2017). The moderate (5.9 M_s), 1967 Pülümür Earthquake is created only 20 cm right-lateral displacement along the 4-km-long section of the Yedisu Fault (Ambraseys 1975). The Kargapazarı Fault which is between the rupture zone of the 1949 event and the KTJ (Fig. 1b) is also interpreted as a ~ 25-km-long seismic gap (Sançar et al. 2009), we believe correctly. Our unpublished field observations suggest ~ 15 cm right-lateral displacement occurred related to the 5.9 M_w 14 June 2020 Karlıova earthquake along the ~ 5-km-long part of the Kargapazarı Fault. As a result of these data, here, we prefer to call the ~ 165-km-long region bearing active faults that were not ruptured by major earthquakes (~ 7.0 M) in the last century as the *Yedisu Seismic Gap* (YSG) (Fig. 1b). All of these faults can be damage sources for the main residential area of the Genç District in the future.

2.2 The Bingöl Seismic Gap of the EAFZ

The instrumental and historical earthquake records evidence that the faults making the EAFZ are capable of creating earthquakes up to ~ 7.2 M_w (Fig. 1b; Table 1) (Pınar and Lahn 1952; McKenzie 1972; Jackson and Mckenzie 1984; Dewey et al. 1986; Ambraseys 1989; Taymaz et al. 1991; Ambraseys and Jackson 1998; Nalbant et al. 2002; Cetin et al. 2003; Tan et al. 2008; Kalafat et al. 2009, 2011; Jamalreyhani et al. 2020; Pousse-Beltran et al. 2020). The destructive May 22, 1971, Bingöl (6.8 M_w) earthquake (Fig. 1b; Table 1) was followed by the first detail mapping of the EAFZ (Arpat and Şaroğlu 1972). Since then, the seismicity of the EAFZ and its Quaternary evolution has been studied intensively (Arpat and Şaroğlu 1975; McKenzie 1976, 1978; Dewey et al. 1986; Muehlberger and Gordon 1987; Westaway 1994; Westaway and Arger 1996; Reilinger et al. 2006; Reilinger and McClusky 2011; Bulut et al. 2012; Duman and Emre 2013; Aktuğ et al. 2016; Yönlü et al. 2017; Khalifa et al. 2018; Akbayram et al. 2021). The EAFZ is a ~ 430-km-long fault zone that lies between the KTJ and Kahramanmaraş (Fig. 1a). The ~ 300-km-long part of the EAFZ ruptured with 7 major earthquakes (6.7 ≤ Ms ≤ 7.2), in the last 160 years (cf., Akbayram et al. 2021 and references therein). Approximately, 108-km-long part of the EAFZ carries a high risk of major earthquakes, namely the Kahramanmaraş and the Bingöl Seismic Gaps (Nalbant et al. 2002; Duman and Emre 2013; Akbayram et al. 2021). The segments of the EAFZ near and around the Genç District, including the Genç Fault Zone (Figs. 1, 2), are parts of the Bingöl Seismic Gap (BSG) (Fig. 1b) (Akbayram et al. 2021). The latest earthquakes in the BSG are the moderate earthquakes (6.1 and 5.6 M_s) that occurred in 2010 (Fig. 1b; Table 1) (Tan et al. 2011). These moderate, however, destructive (Table 1) earthquakes are hardly capable to release the strain accumulated in the BSG (Nalbant et al. 2002), following the 1971 Bingöl earthquake. That's why we think that the faults of the BSG can be damage sources for the main residential area of the Genç District in the future.

2.3 Active Faults formed between the NAFZ and the EAFZ

In addition to the faults of YSG and the BSG, there are other active earthquake damage sources formed at the easternmost sector of the V-shaped intra-plate deformation area of the Anatolian Plate (Fig. 1a, b) (Dewey and Şengör 1979; Sançar et al. 2020). In this deformation area, NW–SE trending dextral faults and NE-SW trending sinistral faults are common (Fig. 1b) (Şengör 1979; Şengör et al. 1985; Emre et al. 2013). The nearest of them to the Genç District are the dextral Sudüğünü Fault (SF)
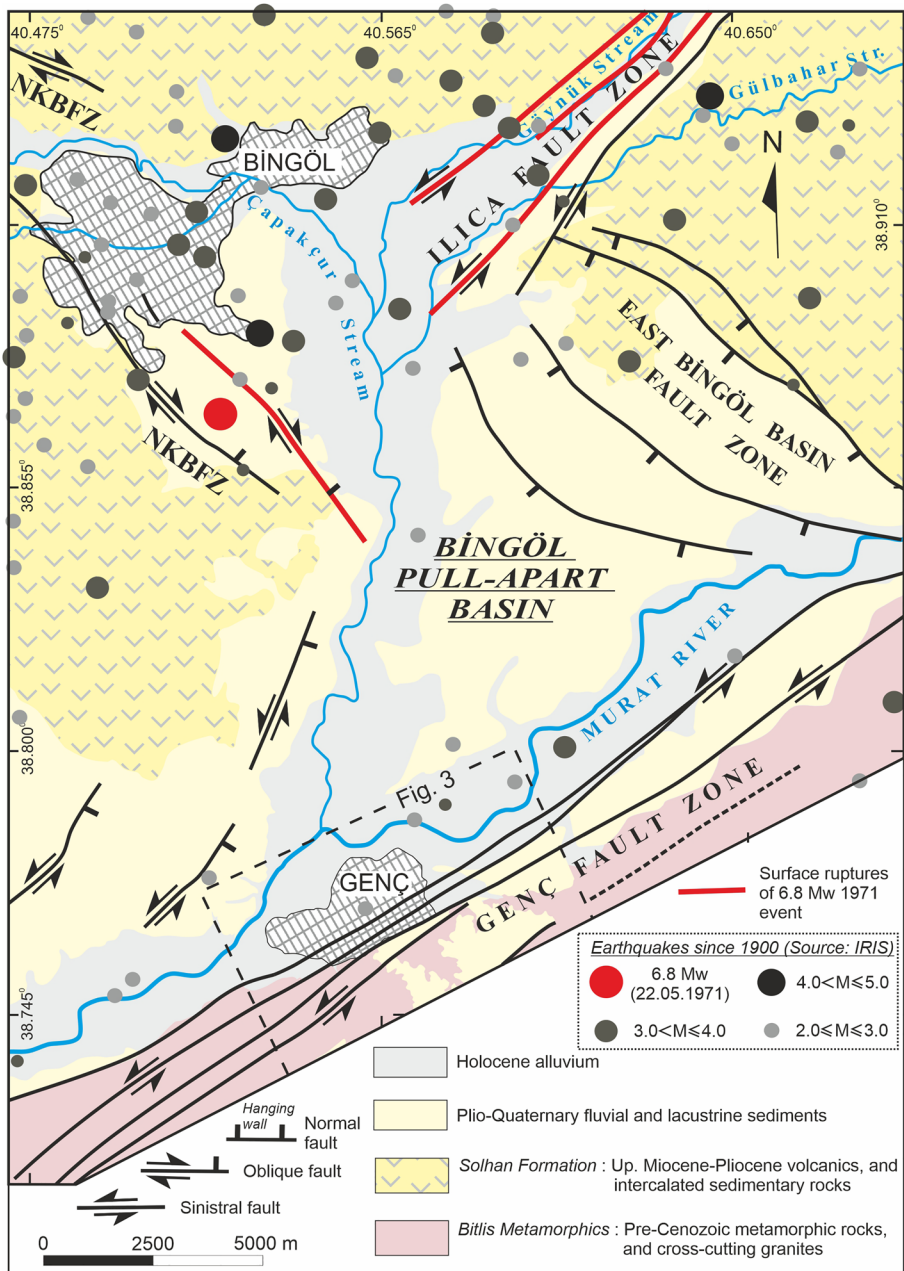
Fig. 2 Geological map of the Bingöl Pull-Apart Basin. The map is compiled from Emre et al. (2013), Herece (2008), Sümengen (2011), Tarhan (2007, 1997), and this study. Earthquakes are from IRIS (2021) database. For the location, see Fig. 1b

and the Nazımiye-Karakoçan-Bingöl Fault Zones (NKBFZ) (Fig. 1b). A devastating earthquake with 6.4 M_s occurred on the Sudüğünü Fault on May 1, 2003, at 03:27 local time (Fig. 1b; Table 1) (Ulusay and Aydan 2005; Akkar et al. 2008; Kalafat et al. 2009; Utkucu et al. 2018). On the Active Fault Map of Turkey (Emre et al. 2013), the NKBZF is evaluated in three separate sections, however, our field observations suggest that all these faults should be considered as a single zone, thus we named them all together as the NKBZF. Studies on the morpho-tectonics of the northeastern part of the NKBZF suggest that this fault zone is tectonically active with at least 25 km cumulative offset (Kara et al. 2013; Sançar 2016). Since the segment structures and the depth of their seismogenic zones are not precisely defined it is hard to assume the earthquake size potential of the NKBZF. However, there is no doubt that it is a major active fault zone, hence, we believe some of its segments can be at least capable of up to 6.3 M_w earthquakes as similar as the Sudüğünü Fault. In addition to all of these faults, there are other active faults such as Yayla and Yenisu Faults at the south of the Genç District (Fig. 1b) (Emre et al. 2013). Although these faults are very close to the Genç District, we have almost no data on their earthquake potential. However, that does not mean that these faults can not be damage sources for the residential area of the Genç District in the future.

2.4 The geology of the Bingöl Pull-Apart Basin

The geological and tectonic evolution of the Bingöl Pull-Apart Basin (BPAB) is controlled mainly by the active faults of the EAFZ (Ilıca, Genç, and East Bingöl Basin Fault Zones) and the NKBFZ (Figs. 1b, 2). Around the BPAB, two geological units crop out at the base of the basin sediments. These units are the Bitlis Metamorphics, and the Solhan Formation (Fig. 2). The Bitlis Metamorphics, cropping-out only in the south of the Bingöl Pull-Apart Basin, is a crystalline complex comprising the Paleozoic–Mesozoic metamorphic rocks and cross-cutting granites (Akay et al., 1998; Boray, 1973; Göncüoğlu and Turhan 1983; Hall 1974; Şaroglu and Yılmaz 1986, 1984; Yılmaz 1975, 1978). The Bitlis Metamorphics is underlined unconformably by the Upper Miocene-Pliocene volcano-sedimentary rocks of the Solhan Formation (Fig. 2) (Şaroglu and Yılmaz 1984, 1986; Yılmaz et al. 1987). The formation begins with conglomerates at the bottom, passing up first into sandstone–siltstone alternations, and then into tuff and agglomerates (Şaroglu and Yılmaz 1984, 1986; Yılmaz et al. 1987). The volcanic rocks of the formation are considered to be the first volcanic products of the neotectonic period in Eastern Anatolia (Şaroglu and Yılmaz 1984, 1986; Yılmaz et al. 1987; Dirik et al. 2003; Emre et al. 2003). The emplacement of the Pliocene volcanic rocks of the formation is interpreted as controlled by the active faulting around the BPAB (Tatar 1986). The basin deposits of the BPAB are usually divided into two units as the Quaternary sediments, and the Holocene alluviums (Fig. 2). The Quaternary sediments are made up of alluvial fan-like terrestrial sediments formed by coarse-grained material along the basin edges, and shallow lacustrine and fluvial sediments with fine-grained clay, sand, and conglomerate in the middle and south of the basin (Şaroglu and Yılmaz 1984, 1986; Tatar 1986; Yılmaz et al. 1987). The sediments near the southeast edge of the BPAB are considered as Pleistocene deposits without precise fossil determination (Şaroglu and Yılmaz 1986). Holocene alluviums deposited along the young rivers such as the Murat River and the Göynük Stream (Fig. 2).

3 New data on the Genç Fault Zone (GFZ), and the soil stratigraphy of the Genç district

Although the segmented nature of the EAFZ has been mapped by many studies (Arpat and Şaroğlu 1972, 1975; Hempton et al. 1981; Muehlberger and Gordon 1987; Barka and Kadinsky-Cade 1988; Şaroğlu et al. 1992; Herece and Akay 1992; Westaway 1994; Herece 2008; Garcia Moreno et al. 2011; Emre et al. 2013; Duman and Emre 2013), there is no consensus on the geometry and the lengths of its faults. This is also the case for the Genç Fault Zone (GFZ) that we partly mapped in this study.

The part of the EAFZ that comprises the GFZ is called the Gökdere Restraining Bend in the Active Fault Map of Turkey (after Emre et al. 2013). The Gökdere Restraining Bend is defined as a 25-km wide, 45 km-long complex fault jog (Duman and Emre 2013) with no active fault zone in the south of BPAB. On the contrary, Herece (2008) mapped a 15-km wide, 30-km-long uplift zone in the north, and another 50-km-long narrow fault zone in the south of the BPAB, in the same region. Our observations support the findings of Herece (2008). This fault zone was also defined partly and named as the Genç Segment by Arpat and Şaroğlu (1975). In this study, we have mapped the faults in the south of the BPAB and realized that they together form a wide fault zone (Fig. 3a). Thus, we prefer the name Genç Fault Zone (GFZ). The geomorphological aspects of some parts of the GFZ are shown in Kıranşan et al. (2021). One of the faults of the GFZ defines the geomorphologic boundary between the young sediments of the BPAB and the uplifted region comprising crystalline rocks of the Bitlis Metamorphics (Fig. 3a, b). This fault also defines the southern boundary of two tectonically induced alluvial fans (Fig. 3a). The mapping of the seismic activity suggests that earthquakes up to 4.0 M_w have occurred along the GFZ (Fig. 2), and tributary streams have deflected along this fault zone (Fig. 3a). The longest stream deflections have been observed along the northernmost fault of the GFZ in the NE of our mapping area (Fig. 3a). This fault, cutting mainly through the Holocene alluvium shown in red in our geological map (Fig. 3a), can be the seismic source of a possible future earthquake. All of these observations suggest that faults become younger towards the northwest in the GFZ. The northwestward younging direction interpretation is also supported by the geomorphological position of the faults (Fig. 3b).

In this study, we have also reviewed four geotechnical core logs to give insight into the sediment type of the southern part of the BPAB. The logs, collected from different topographic levels of the Genç District (Fig. 3a, b), were kindly supplied by the Granit Mühendislik Ltd. Even tough these logs were not taken along a straight-line (Fig. 3a), we have correlated these logs and created a correlation-based geological cross-section (Fig. 3b) to understand stratigraphical changes from the bottom to the top of the southern part of the BPAB. These four core logs together show typical sedimentary features of a fan delta. At the southernmost core log (Fig. 3a, b, Well 4), the unconformity between the metamorphic basement rocks and the pale brown silt-dominated layers with minor clay and sand intercalations of the Holocene Alluvium had been cut (Fig. 3b). In the other three ~20-m-deep core logs, the unconformity and the metamorphic basement could not observe (Fig. 3b). The absence of the basement in shallow depths, unlike Well 4, suggests that northwestward deepening of the basin is controlled by faulting as can be followed in the geological cross-section made by the core logs (Fig. 3b). At the base of the other core logs, greyish brown gravel-boulder dominated layers with sand and minor clay intercalations have been determined (Fig. 3b). Pale brown sand-dominated layers with less clay and minor gravel conformably overlie the gravel-boulder-dominated lowermost layers in Wells 1 and 3 (Fig. 3b).
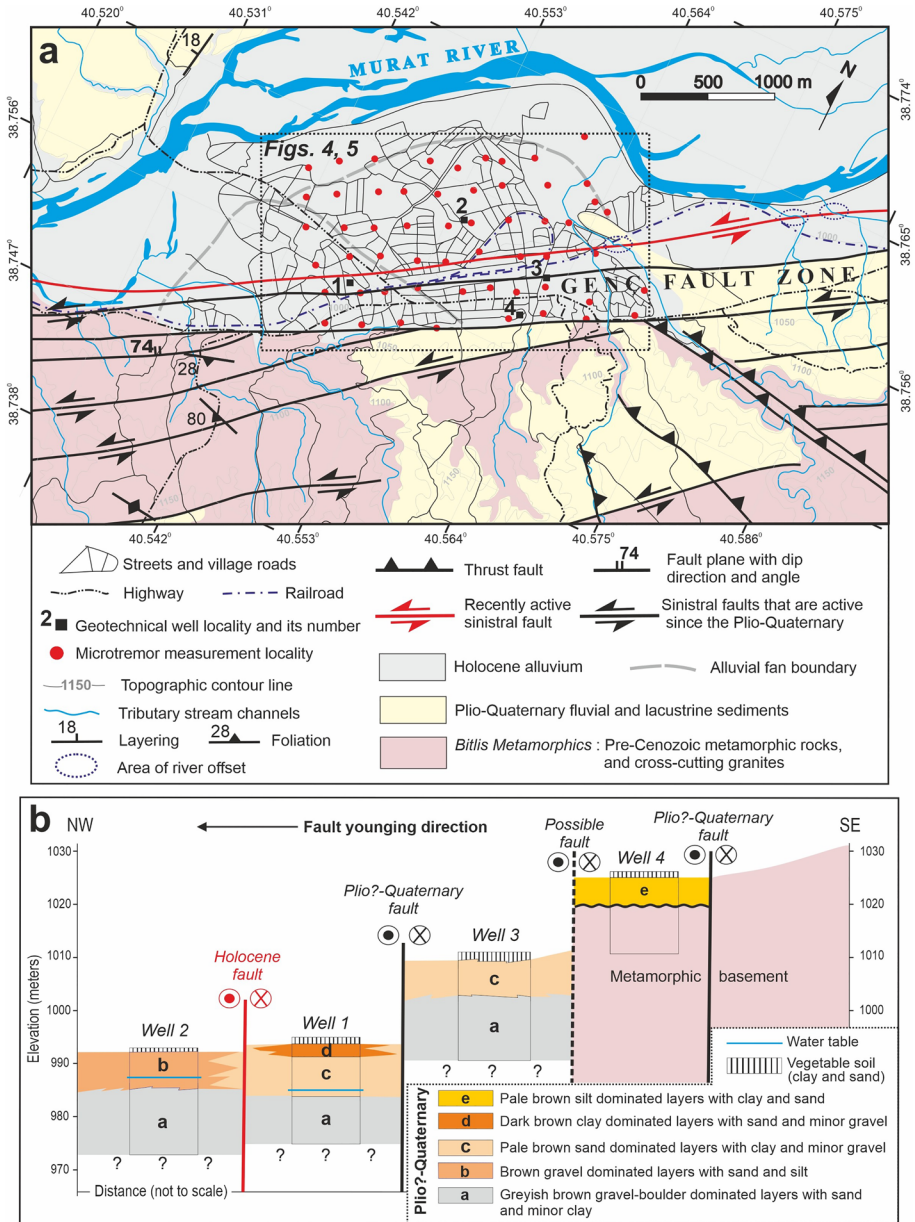
Fig. 3 a Geological map of the Genç District with streets, highways, railroads of the main residential area, and 59 microtremor measurement sites (red dots). For the location, see Fig. 2. **b** Simplified soil-geological cross-section based on the geotechnical well data and the geological map. For the location of the geotechnical wells, see **a**

Dark brown clay-dominated layers with less sand and minor gravel overlie conformably to the sand-dominated layers in Well 1. In Well 2, gravel-boulder-dominated layers are

directly overlain by brown gravel-dominated layers with lesser sand and silt. Water table only observed in Wells 1 and 2 at the lowermost, northwestern part of our cross-section.

4 Single station microtremor survey and methods

We conducted a microtremor survey to define the dynamic sub-surface characteristic of the Genç District. The data were collected with Guralp CMG-6TD seismometers at 59 sites with approximately 250 mt intervals (Figs. 3a, 4). The sampling frequency was 100 Hz, and the measurement time ranges from 20 to 50 min, depending on the noise level of the measurement point. We used a band-pass filter in the range of 0.05–20 Hz. Also, the 50 s window and 5% cosine taper were applied.

We have followed the "Nakamura method" known as the single-station microtremor method (or H/V spectral ratios method; HVSR) to obtain the predominant period (or frequency) of soil, and amplification of ground motions influenced by surface layer (Nakamura and Saito 1983; Nakamura 1989, 2000, 2019). Microtremors are Rayleigh-type
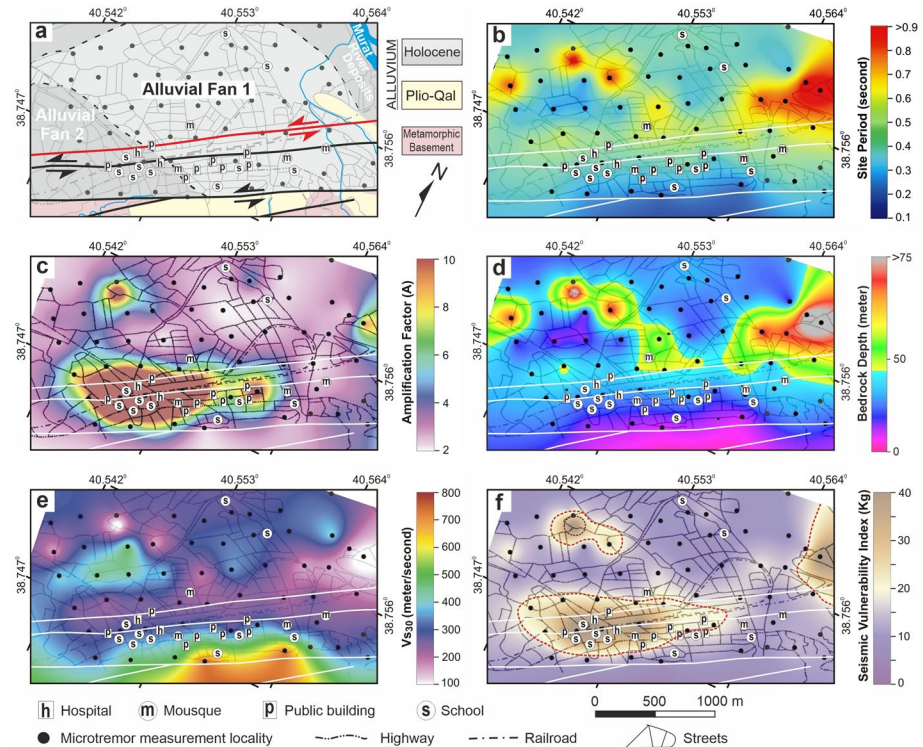
Fig. 4 **a** The geological, **b** the average dominant period (*T*), **c** the soil amplification factor (*A*), **d** the bedrock depth (*BD*), **e** the shear wave velocity (*Vs₃₀*), and **f** the seismic vulnerability index (*Kg*) maps of the single-station microtremor survey area with streets, highways, railroads of the Genç District. The black dots indicate the measurement sites. The faults are shown as black or red lines in **a**, and white in others. The red fault in **a** is the most active fault. The location of hospitals, public buildings (e.g. municipality, security buildings), schools, and mosques are also shown in each figure. See the text for detailed explanations. For the location, see Fig. 3a

waves created by surface sources (Nogoshi and Igarashi 1970a, b, 1971; Nakamura 1989). Rayleigh waves are affected by both horizontal and vertical movements (Nogoshi and Igarashi 1970a, b, 1971; Nakamura 1989). This method assumes that microtremors are formed from vibrations from sources near the surface (Nakamura 1989, 2000, 2019). According to this method, while the vertical components are not affected by changes depending on the density and velocity of the underground layers the horizontal components are largely affected. Therefore, the soil transfer function is obtained by dividing the horizontal component spectrum to the vertical component spectrum, as shown in Eq. 1 (Nakamura 1989). In Eq. 1, HVSR is the amplification factor, NS and EW are amplitude spectrums of the North–South and East–West component of the record, and V is amplitude spectrum of the vertical component.

$$\text{HVSR} = \frac{\sqrt{\left(\text{NS}^2\right) + \left(\text{EW}^2\right)}}{V} \tag{1}$$

As a result of our single station microtremor (HVSR) survey, we have prepared the distribution maps of different soil parameters of the Genç District. These soil parameters are; (1) dominant period (T), (2) soil amplification factor (A), (3) the bedrock depth (BD), (4) shear wave velocity for the first 30 m (Vs_{30}), (5) seismic vulnerability index (Kg). Then we have calculated (6) shear strain distribution for three bedrock acceleration values; 0.25, 0.50, and 0.75 g. Below we introduce the calculation of each soil parameter and shear strain distribution for bedrock acceleration values.

4.1 Calculation of dominant period (*T*), and amplification factor (*A*)

In this study, we obtained the dominant period (T), and amplification factor (A) values with the single-station method of (Nakamura 1989, 2000, 2019). When the dominant period value decreases, the strength of the soil increases, and as the dominant period value increases, the strength of the soil decreases. The *H/V* amplitude reached the higher values at soft soil sites, and it refers to the amplification factor (Nakamura and Saito 1983; Nakamura 2000, 2019). Whereas, the *H/V* ratio becomes low (~ 1) in the compact rigid soil meaning there is little or no amplification (Nakamura and Saito 1983; Nakamura 2000, 2019). For this reason, the Nakamura method can be accepted as an evaluation technique for both resonance frequency and an amplification factor (Nakamura 2019). We obtained the *H/V* spectra by applying the single station microtremor method to seismic noise records measured at 59 points. The maximum amplitude of these spectra represents the amplification factor, and the frequency corresponding to the maximum amplitude represents the dominant period.

4.2 Empirical calculation of bedrock depth

Bedrock depth can generally be defined using the shear wave velocity (*Vs*) in geothecnical studies. However, it can also be calculated using empirical correlations developed between the dominant frequency and bedrock depth in cases where there is no direct *Vs* information depending on the depth obtained for the study area (cf., Ibs-Von Seht and Wohlenberg 1999; Parolai et al. 2002; Pamuk 2019; Pamuk and Ozer 2020; Aydın et al. 2021). In the present study, we use the most widely used empirical correlation equations (Eqs. 2–4) to calculate bedrock depth from single-station microtremor measurements (D_D is from Dinesh

et al. 1997; D_I is from Ibs-Von Seht and Wohlenberg 1999; D_P is from Parolai et al. 2002). Then, we have taken the arithmetic average of three different values to increase the reliability of the bedrock depth calculated by different equations given below where f_r is the dominant frequency.

$$D_D = 58.29 * f_r^{-0.95} \tag{2}$$

$$D_P = 108.0 * f_r^{-1.551} \tag{3}$$

$$D_I = 96.0 * f_r^{-1.388}. \tag{4}$$

4.3 Shear wave velocity (Vs_{30}) determination

Vs_{30} (average Vs for the first 30 m below surface) is usually obtained by using seismic methods such as MASW, ReMi, SPAC, seismic refraction (Park et al. 1999, 2007; Louie 2001; Okada and Suto 2003; Okada 2006). However, when there are no seismic measurements, Vs_{30} prediction maps can be made using empirical correlations developed between the soil dominant period and Vs_{30} (Stanko and Markušić 2020). The Vs_{30} maps obtained by empirical correlations in geotechnical analyses, provide preliminary information about the Vs structure of the study area. The Vs_{30} map of the study area was formed by using the period values obtained from the Nakamura method, and Eq. 5 of Stanko and Markušić (2020). In this equation, Vs_{30} is the average shear wave velocity, and T is the dominant period value.

$$V_{s30} = e^{\left(5.34 + 0.46 * \ln\left(\frac{1}{T}\right)\right)}. \tag{5}$$

4.4 Seismic vulneribility index (Kg) calculation

Nakamura (1997, 2000, 2019) has shown a relationship between the Kg and maximum amplitude-frequency values. Thus, it is possible to determine the vulnerable places of a selected area before a devastating earthquake. In the present study, the Kg value of each measurement point is calculated by Eq. 6. In this equation, A is the amplification factor and the T is the dominant period value.

$$Kg = A^2 * T. \tag{6}$$

4.5 Soil dynamic features: modelling shear strain distribution for choosen bedrock acceleration values

Estimating the values of shear deformation that may occur in the strata near the surface during an earthquake is crucial for damage reduction. Shear strains (γ_e) that may occur during strong soil movement can be calculated using the seismic vulnerability index (Kg), the largest acceleration value of the bedrock (a_{max}), and the shear wave velocity value of bedrock ($V_b = 760$ m/s) for the soil surface as in Eq. 7 (Nakamura 1996, 1997, 2000). In this equation,

e refers to the coefficient defining the efficiency of strong ground motion. The shear strain has been calculated with the acceptance of $e = 60\%$.

$$\gamma_e = \mathrm{Kg} * \frac{e}{(\pi^2 * V_b)} * a_{max} \qquad (7)$$

In Eq. 7, a_{max} refers to the acceleration value that can occur on the bedrock due to an earthquake denominated in gal. In this study, we have chosen three acceleration values (a_{max}—PGA in bedrock) as 0.25 g, 0.50 g, 0.75 g for the shear strain analysis. We have chosen these values because the Disaster and Emergency Management Authority's Earthquake Hazard Map of Turkey (AFAD 2019) suggests that the expected maximum peak ground acceleration value for a return period of 475 years would be 0.625 g in the study area.

The behavior of soils according to shear strain values changes between elastic to plastic (Table 2) (Ishihara 1996; Nakamura 1997). As the shear strain value increases, the elastic properties of the soils disappear and the possibility of damage to the structures located on them increases (Table 2).

5 Results and discussion

As outlined in the previous sections, the Genç District is surrounded by the major seismic sources that are capable of disastrous earthquakes such as faults of Yedisu and Bingöl Seismic Gaps, and Nazımiye-Bingöl-Karakoçan Fault Zone and some other individual faults (e.g., Yayla and Yenisu Faults) (Fig. 1b). Most of these faults are away from the Genç District tens of kilometers. However, the Genç Fault Zone of Bingöl Seismic Gap is cutting through the Genç District. Thus, the GFZ poses the greatest danger for the residential area of the Genç District, comparing the other surrounding faults (Figs. 3a, 4a). Some stress transfer is likely to have taken place to the Bingöl Seismic Gap after the 1971 (M 6.8) Bingöl earthquake (Nalbant et al. 2002). This stress may soon be released by some fault (or faults) in the future (Nalbant et al. 2002). Accordingly, the GFZ can be the host of the next big earthquake in the future and will severely damage the Genç District related to its location and loose soil structure of District. Not only many residential buildings but also public buildings such as schools, hospitals, mosques, and district governorship buildings stay over the active fault of GFZ (Fig. 4a). Geodetic data also suggested high strain values in Bingöl, hence a need for field-specific multidisciplinary studies in this area (Yavasoglu 2015). According to the slip model of May 1, 2003, the Bingöl earthquake rupture was unilateral towards Genç District with a peak displacement of about 55 cm (Utkucu et al. 2018). The coulomb analysis also showed high-stress accumulation for the Genç District (Poyraz et al. 2019).

When it comes to the possible damage related to the seismic sources kilometers away from the Genç District, we must focus on our distribution maps of different soil parameters formed as results of our microtremor survey and analyses (Fig. 4). In our survey area, *the dominant period values* (T) range from 0.1 to 2.0 s (Fig. 4b). The highest values ($T \geq 0.9$ s) were obtained in the northeast and northwest of the study area (Fig. 4b). The lowest values ($T < 0.2$ s) were

Table 2 Strain dependence of dynamic properties of soil (from Ishihara 1996)

Size of Strain γ	10^{-6}	10^{-5}	10^{-4}	10^{-3}	10^{-2}	10^{-1}	
Phenomena		Wave, Vibration		Crack, Settlement		Landslide, Soil Compaction, Liquefaction	
Dynamic Properties		Elasticity		Elasto-Plasticity		Collapse	
						Repeat- Effect, Speed- Effect of Loading	

obtained in the south (Fig. 4b) because here the basement rocks are either on the surface and/ or underlain by very thin unconsolidated sediments (Fig. 4a). In the central parts, where the youngest faults of the GFZ are mapped (Figs. 3a, 4a), the T values are generally between 0.4 and 0.6 s. In the survey area, the *amplification factor values* (A) range between 2 to 10, and are greater than 4 in general (Fig. 4c). The highest A values (8–10) were obtained in three areas (Fig. 4c). The most important of them is at the southwestern-central part of the survey area that occupies a ~2-km-long area with a maximum width of 0.6 km (Fig. 4c). This biggest area of high A comprises most of the schools, mosques, public buildings, and hospitals hence carrying a high risk of disaster. The second noteworthy area of the high A is at the north of the survey area which is relatively small and there are almost no residential buildings over here. Generally, high soil amplification is observed at low frequencies in loose units (Yalçınkaya 2010). The *average bedrock depth* (BD) in the study area ranges from 0 to 180 m (Fig. 4d). Please note that $75 < BD < 180$ m is shown in grey in Fig. 4d. We have obtained the shallowest bedrock depth values ($BD < 12$ m) in the south of the study area that is compatible with the geological map (Figs. 3a, 4a). The deepest bedrock depth values ($BD > 75$ m) were obtained at the northeast and northwest of the study area. Bedrock depth in the north and south-east of the study area is generally between 10 and 25 m (Fig. 4d). The projection of our fault map over the BD map suggests that the northernmost youngest fault of the GFZ (Figs. 3a, 4a) defines the boundary of sudden bedrock deepening in its central and north-eastern part (Fig. 4d). That would be interpreted that along the GFZ, pull-apart basins and ridges are recently forming. The *average shear wave velocity for the first* 30 m *below surface* (Vs_{30}) *values* range from 100 to 800 m/s in the survey area (Fig. 4e). The highest Vs_{30} values ($500 \leq Vs_{30} \leq 800$ m/s) were obtained in the south of the study area (Fig. 4e) as expected because of the existence of the crystalline rocks in this region (Fig. 4a). There is a region with ~400 m/s in the north-western part of the survey area (Fig. 4e) overlapping shallow (~25 m) bedrock depth values (Fig. 4d). The $Vs_{30} \leq 300$ m/s values were obtained along most of the loose sediments of the Bingöl Pull-Apart Basin (Fig. 4e) cropping out over ~40-m-deep bedrocks (Fig. 4d). We have also checked Vs_{30} values obtained by seismic methods in available geotechnical reports (see their locations on Fig. 3a) and see a good correlation with our results. The *seismic vulnerability index values* (Kg) range between 1 and 50 in the survey area (Fig. 4f). Our Kg distribution map is represented mainly by two colors (Fig. 4f). The brown sections show areas where Kg is greater than 20, and the purple sections show areas where Kg is less than 20. There are three areas of high Kg (>20) in the east, northwest, and southwest of the study area (Fig. 4f). In the areas of $Kg > 20$, bedrock depth is less than ~25 m, and in the areas of low $Kg < 20$, bedrock depth is greater than ~30 m, the dominant period values are greater than 0.5 s, and the amplification factor values are greater than 3 (Fig. 4b–f). When fault and soil parameter maps are evaluated together with the location of the Genç District's buildings the area that may be at high risk of destruction during an earthquake would be the largest, central area of high Kg (>20) shown in Fig. 4f. This area includes two hospitals, five schools, and almost all governmental public buildings of the Genç District (Fig. 4f).

5.1 Shear strain distribution scenarios

Using all of the data, we have also calculated the *shear strain values* (γ_e) of the study area for three chosen *acceleration values* (a_{max}—PGA in bedrock) as 0.25 g, 0.50 g, 0.75 g to make three different damage scenarios that we introduce as maps (Fig. 5). The maximum peak ground acceleration value is reported as 0.55 g after the 6.4 M_w 2003 Bingöl earthquake (Akkar et al. 2008). Recently, the average peak ground acceleration value was
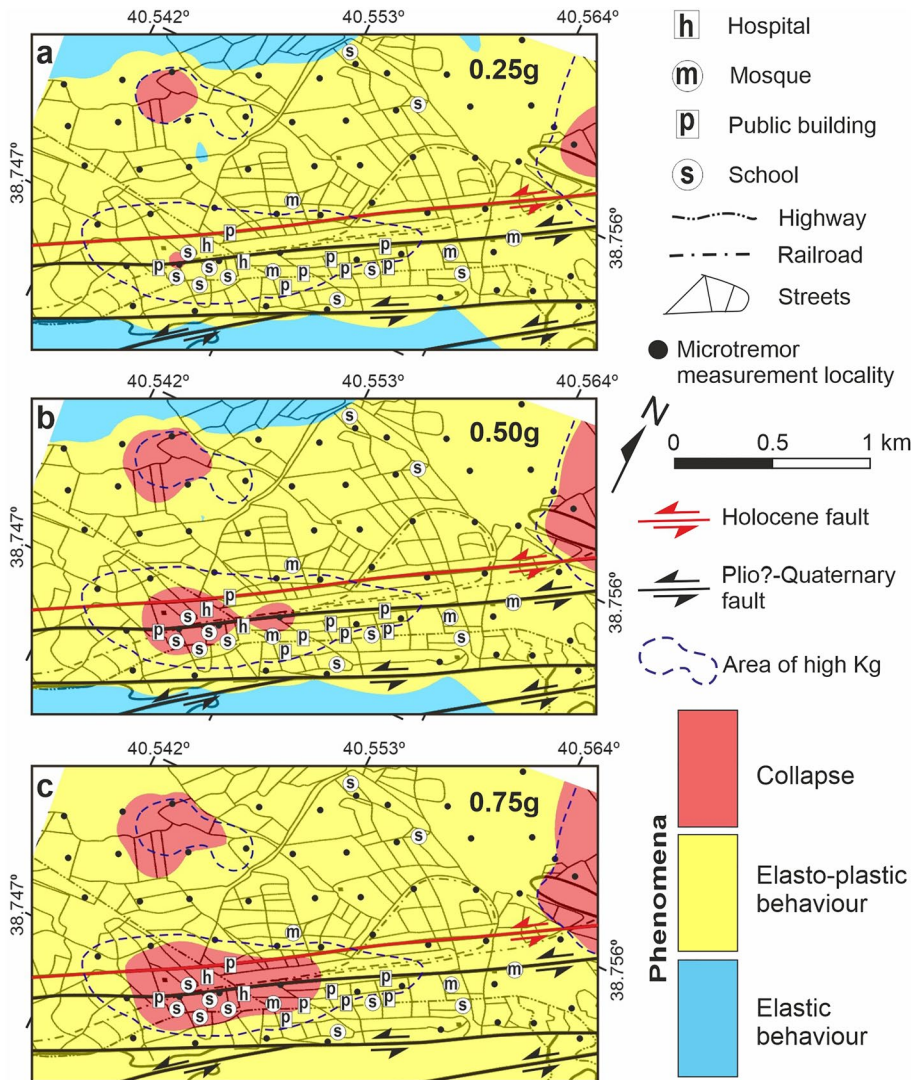
Fig. 5 The shear strain distribution maps for **a** 0.25 g, **b** 0.50 g, and **c** 0.75 g bedrock acceleration values. See the text for detailed explanations. For the location, see Fig. 3a

calculated as 0.58 g with a probability of %10 exceeding in 50 years for the Bingöl Province (Balun et al. 2020). Additionally, the Disaster and Emergency Management Authority's Earthquake Hazard Map of Turkey (AFAD 2019) suggests that the expected maximum peak ground acceleration value for a return period of 475 years would be 0.625 g in the study area. Thus, we have chosen the 0.25 g, 0.50 g, 0.75 g values to model possible damages which are either below or just above the 0.625 g.

For the shear strain distribution calculated by 0.25 g *bedrock-acceleration-value,* elastic behavior is observed in the south and the northwest of the study area (Fig. 5a) where the

bedrocks are either exposes on surface or shallow (~ 25 m). In three areas, we have defined plastic dynamic behavior (or collapse) of soils (red areas in Fig. 5a). The largest, plastically behaving areas occur in the two relatively small areas of high *Kg* values documented (Fig. 5a). We have mapped the smallest area with plastic behavior of soil in the SW part of the largest area of high *Kg* (> 20) (Fig. 5a), in the central part of the Genç District. In other areas, soil behaves elasto-plastically if a 0.25 g bedrock acceleration value occurs (yellow areas in Fig. 5a) related to an earthquake.

When the shear strain distribution exceeds 0.50 g *bedrock-acceleration-value,* we modeled elastic behavior in areas where the bedrock comes to the surface or is mapped shallower than 25 m, just like the 0.25 g value (Fig. 5b). On the other hand, at 0.50 g scenario, the area of plastically behaving soil increases significantly, in areas with *Kg* > 20. The most significant expansion in plastic behavior areas was detected in the largest high-*Kg* area of the Genç District center, where the school, hospital, and other important public buildings are located (Fig. 5b).

When the shear strain distribution exceeds 0.75 g *bedrock-acceleration-value,* the soil does not behave elastically anywhere in the study area (Fig. 5c). In this scenario, the area of plastic-behaving soils covers a ~ 1-km-long and ~ 350-m-wide area, in the central part of the Genç District, along the active faults of the GFZ (Fig. 5c). This striking result shows that if g values of 0.75 or greater occur during an earthquake in the center of Genç district, a high rate of deformation will develop in the soil.

In summary, our earthquake damage prediction scenarios evidence that as the bedrock acceleration values increase, the area of soil plastic behavior expands, and the area of soil elastic and elasto-plastic behavior shrinks linearly (Fig. 5). If the average expected peak ground acceleration value (0.55–0.625 g) (Akkar et al. 2008; AFAD 2019; Balun et al. 2020) is exceeded during an earthquake significant damage would be inevitable for the central part of the Genç District (Fig. 5b, c). Our study shows that most of the public structures of the Genç District, such as hospitals, schools, municipality buildings, and mosques are unfortunately established over major active faults and soils showing high seismic vulnerability (Figs. 3, 4, 5).

6 Conclusions

The Genç District of the city of Bingöl has been established over three parallel SW-NE trending left-lateral faults of the Genç Fault Zone (GFZ) which is a part of Bingöl Seismic Gap of the East Anatolian Fault Zone. The most active fault segment of the GFZ cuts through the central part of the District where almost all of the public buildings (schools, hospitals, mosques, municipality buildings) are located. The District is established over the loose alluvial soils of the southern section of the Bingol Pull-Apart Basin. The contact between the basin sediments and the crystalline basement rocks is also a fault of the GFZ. The average dominant period (*T*) values of the soil under the District are between 0.1 and 2.0 s, and the average soil amplification factor (*A*) is greater than 4. The lowest *T* values (< 0.2 s) and the highest *A* values (8–10) were obtained in the southwestern-central part of the District. The bedrock becomes deeper from 0 to ~ 180 m from the crystalline basement in the south towards the basin sediments in the north. The Vs_{30} values range from 100 to 800 m/s in the survey area, the lowest values (≤ 300 m/s) were obtained along most of the loose sediments cropping out over ~ 40-m-deep bedrocks along with the District. The vulnerability index value (*Kg*) is between 1 and 50 in general, very high *Kg* values (> 20)

were obtained in the southwestern-central part and the eastern part of the District. The calculation of shear strain distribution for three bedrock acceleration values (0.25, 0.50 g, and 0.75 g) suggests that if the acceleration values exceeded to average reported peak ground acceleration value (0.55–0.625 g) during an earthquake, loose soil under the central part of the Genç District behaves plastically. Hence, in the central part of the District, comprising almost all of the schools, hospitals, mosques, municipality buildings, major railroads, and highways, significant damage will be inevitable.

Author contributions All authors contributed to the study conception and design. Material preparation, data collection and analysis were performed by all authors. The first draft of the manuscript was written by KA and all authors commented on previous versions of the manuscript. All authors read and approved the final manuscript.

Declarations

Conflict of interest The authors have no relevant financial or non-financial interests to disclose.

References

Adnan A, Ramli M, Abd Razak S (2015) Disaster management and mitigation for earthquakes: Are we ready? In: 9th Asia Pacific structural engineering and construction conference (APSEC2015), pp 34–44

AFAD (2019) Earthquake risk map of Turkey. https://deprem.afad.gov.tr/deprem-tehlike-haritasi?lang=en

AFAD (2021) The online earthquake catalog of Ministry of Interior Disaster and Emergency Management Presidency of Turkey. http://www.deprem.gov.tr

Akay E, Göncüoğlu M, Turhan N (1998) 1/100,000 ölçekli Açınsama Nitelikli Türkiye Jeoloji Haritaları Serisi, Muş H33 Paftası. Maden Tetkik ve Arama Genel Müdürlüğü (MTA), Ankara, Turkey

Akbayram K, Kıranşan K, Özer Ç, Varolgüneş S (2021) The surface deformation of the 2020 Doğanyol-Sivrice earthquake (Mw 6.8) and the earlier events suggest Mw ˂7.0 earthquakes do not create significant surface slip along the East Anatolian Fault Zone

Akkar S, Boore DM, Gülkan P (2008) An evaluation of the strong ground motion recorded during the May 1, 2003 Bingol Turkey, earthquake. J Earthq Eng 9:173–197. https://doi.org/10.1080/1363246050 9350538

Aktuğ B, Ozener H, Doğru A et al (2016) Slip rates and seismic potential on the East Anatolian Fault System using an improved GPS velocity field. J Geodyn 94–95:1–12

Allen CR (1969) Active faulting in Northern Turkey. Pasadena, CA, USA

Altuncu Poyraz S, Aksarı D, Ergün T et al (2019) The December 2nd, 2015 Bingöl, Eastern Anatolia-TURKEY, earthquake (Mw = 5.3): a rupture on optimally oriented fault plane. J Asian Earth Sci 173:88–97. https://doi.org/10.1016/j.jseaes.2018.12.019

Ambraseys N (1970) Some characteristic features of the Anatolian fault zone. Tectonophysics 9:143–165

Ambraseys N (1975) Studies in historical seismicity and tectonics. Geodyn Today 7:1

Ambraseys N (1989) Temporary seismic quiescence: SE Turkey. Geophys J Int 96:311–331. https://doi.org/10.1111/j.1365-246X.1989.tb04453.x

Ambraseys N, Jackson J (1998) Faulting associated with historical and recent earthquakes in the Eastern Mediterranean region. Geophys J Int 133:390–406. https://doi.org/10.1046/j.1365-246X.1998.00508.x

Andrieux J, Over S, Poisson A, Bellier O (1995) The North Anatolian Fault Zone: distributed Neogene deformation in its northward convex part. Tectonophysics 243:135–154

Andrus R, Stokoe K II (2000) Liquefaction resistance of soils from shear-wave velocity. J Geotech Geoenviron Eng 126:1015–1025

Arpat E, Şaroğlu F (1972) The East Anatolian Fault System: thoughts on its development. Maden Tetk Ve Aram Derg 78:33–39

Arpat E, Şaroğlu F (1975) Recent tectonic activities in Turkey. Bull Geol Soc Turkey 18:91–101

Ataman G, Buket E, Çapan U (1975) Kuzey Anadolu Fay zonu bir Paleo-Benioff zonu olabilir mi? Maden Tetk Ve Aram Derg 84:112–118

Aydın U, Pamuk E, Özer Ç (2021) Investigation of soil dynamic characteristics at seismic stations using H/V spectral ratio method in Marmara Region, Turkey. Nat Hazards 110:1–20

Balun B, Nemutlu O, Benli A, Sarı A (2020) Estimation of probabilistic hazard for Bingol province, Turkey. Earthq Strcut 18:223–231

Barka A (1992) The North Anatolian fault zone. Ann Tectonicae 6:164–195

Barka A, Kadinsky-Cade K (1988) Strike-slip fault geometry in Turkey and its influence on earthquake activity. Tectonics 7:663–684. https://doi.org/10.1029/TC007i003p00663

Barka A, Toksoz M, Gülen L, Kadinsky-Cade K (1987) Kuzey Anadolu Fayının Doğu Kesiminin Segmentasyonu, Sismisitesi ve Deprem Potansiyeli. Yerbilimleri 14:337–352

Boray A (1973) The structure and Metamorphism of the Bitlis Area. University of London, London

Bulut F, Bohnhoff M, Eken T et al (2012) The East Anatolian Fault Zone: Seismotectonic setting and spatiotemporal characteristics of seismicity based on precise earthquake locations. J Geophys Res 117:1–16. https://doi.org/10.1029/2011JB008966

Cavalié O, Jónsson S (2014) Block-like plate movements in eastern Anatolia observed by InSAR. Geophys Res Lett 41:26–31. https://doi.org/10.1002/2013GL058170

Cetin H, Güneyli H, Mayer L (2003) Paleoseismology of the Palu-Lake Hazar segment of the East Anatolian Fault Zone, Turkey. Tectonophysics 374:163–197. https://doi.org/10.1016/j.tecto.2003.08.003

Demirtaş R (2019) 12 Mart 2005 (M = 5.6), 14 Mart 2005 (M = 5.9) ve 24 Mart 2005 (M = 5.4) Karlıova (Bingöl) Depremleri. Ankara

Dewey J, Şengör A (1979) Aegean and surrounding regions: complex multiplate and continuum tectonics in a convergent zone. Geol Soc Am Bull 90:84–92

Dewey J, Hempton M, Kidd W et al (1986) Shortening of continental lithosphere: the neotectonics of Eastern Anatolia—a young collision zone. Geological Society. Special Publications, London, pp 1–36

Dinesh B, Nair G, Prasad A et al (1997) Relation between sedimentary layer thickness and fundamental frequency of the H/V spectra for Bangalore city. Curr Sci 1997:1073–1077

Dirik K, Yürür Y, Demirbağ A (2003) 1 Mayıs 2003 Çimenli (Bingöl) Depremi Değerlendirme Raporu, Ankara, Turkey

Duman TY, Emre Ö (2013) The East Anatolian Fault: geometry, segmentation and jog characteristics. Geological Society. Special Publications, London, pp 495–529

Emre Ö, Herece E, Doğan A, et al (2003) 1 Mayıs 2003 Bingöl depremi değerlendirme raporu. Ankara, Turkey

Emre Ö, Duman T, Özalp S, et al (2013) Active fault map of Turkey with an explanatory text 1:1.250.000 scale, Special Publication Series - 30. General Directorate of Mineral Research and Exploration (MTA), Turkey

Ergintav S, Reilinger R, Çakmak R et al (2014) Istanbul's earthquake hot spots: geodetic constraints on strain accumulation along faults in the Marmara seismic gap. Geophys Res Lett 41:5783–5788. https://doi.org/10.1002/2014GL060985

Eyidogan H, Guclu U, Utku Z, Degirmenci E (1991) Türkiye Büyük Depremleri Makro-Sismik Rehberi (1900–1988). ITU Maden Fakultesi Jeofizik Muhendisligi Bolumu, İstanbul

Garcia Moreno D, Hubert-Ferrari A, Moernaut J et al (2011) Structure and recent evolution of the Hazar Basin: a strike-slip basin on the East Anatolian Fault, Eastern Turkey. Basin Res 23:191–207. https://doi.org/10.1111/j.1365-2117.2010.00476.x

Göncüoğlu MC, Turhan N (1983) New results on the age of Bitlis Metamorphics. Bull Miner Res Explor 95–96:44–48

Hall B (1974) The structure and petrology of an ophiolitic melange near mutki, Bitlis Province. University of London, Turkey

Hempton M, Dewey J, Şaroğlu F (1981) The East Anatolian transform fault : along strike variations in geometry and behavior. Eos Trans Am Geophys Union 62:393

Herece E, Akay E (1992) Karlıova-Çelikhan arasında Doğu Anadolu Fayı. In: 9th petroleum congress of Turkey, pp 361–372

Herece E (2008) Atlas of East anatolian fault—special publication series, 13. General Directorate of Mineral Research and Exploration (MTA), Turkey, Ankara

Hubert-Ferrari A, Armijo R, King G et al (2002) Morphology, displacement, and slip rates along the North Anatolian Fault. Turk J Geophys Res 107:2235. https://doi.org/10.1029/2001JB000393

Ibs-Von Seht M, Wohlenberg J (1999) Microtremor measurements used to map thickness of soft sediments. Bull Seismol Soc Am 89:250–259

IRIS—Incorporated Research Institutions for Seismology (sponsored by National Science Foundation of USA). https://www.iris.edu/hq/

Ishihara K (1996) Soil behaviour in earthquake geotechnics. Clarendon Press, Oxford

İyisan R, Haşal M (2011) The basin edge effect on dynamic response: dinar basin model. Tek Dergi 22:1499–1518

Jackson J, Mckenzie D (1984) Active tectonics of the Alpine-Himalayan Belt between western Turkey and Pakistan. Geophys J R Astron Soc 77:185–264

Jamalreyhani M, Büyükakpınar P, Cesca S et al (2020) Seismicity related to the eastern sector of Anatolian escape tectonic: the example of the 24 January 2020 Mw 6.77 Elazığ-Sivrice earthquake. Solid Earth Discuss. https://doi.org/10.5194/se-2020-55

Kalafat D, Kekovalı K, Güneş Y et al (2009) A catalogue of source parameters of moderate and strong earthquakes for Turkey and its surrounding area (1938–2008). Boğaziçi University, Kandilli

Kalafat D, Güneş Y, Kekovalı K et al (2011) A revised and extented earthquake cataloque for Turkey since 1900 (M ≥ 4.0), 1049th edn. Boğaziçi University, Kandilli Observatory and Earthquake Research Institute, İstanbul

Kara K, Sançar T, Zabcı C (2013) Morphologic and morphotectonic characteristics of the nazimiye fault zone, Eastern Turkey. In: EGU General Assembly 2013. Vienna, pp EGU2013–8105

Kawase H (2003) Site effects on strong ground motions. In: Lee WHK, Kanamori H, Jennings P, Kisslinger C (eds) International handbook of earthquake & engineering seismology, Part B, 81st edn. Academic Press, pp 1013–1030

Kayen R, Moss R, Thompson E et al (2013) Shear-wave velocity–based probabilistic and deterministic assessment of seismic soil liquefaction potential. J Geotech Geoenvironm Eng 139:407–419

Ketin I (1948) Über die tektonisch-mechanischen Folgerungen aus den großen anatolischen Erdbeben des letzten Dezenniums. Geol Rundschau 36:77–83. https://doi.org/10.1007/BF01791916

Ketin I (1957) Kuzey Anadolu Deprem Fayı. İstanbul Tek Üniversitesi Derg 15:49–52

Ketin I (1969) Über die Nordanatolische horizontal verschiebung. Bull Miner Res Explor 72:1–27

Khalifa A, Çakir Z, Owen LA, Kaya Ş (2018) Morphotectonic analysis of the East Anatolian Fault, Turkey. Turk J Earth Sci 27:110–126. https://doi.org/10.3906/yer-1707-16

Kıranşan K, Akbayram K, Avci V (2021) Effects of active tectonism on geomorphological structure in bingöl basin and its surroundings. Gümüşhane Üniversitesi Sos Bilim Enstitüsü Elektron Derg 12:1110–1129

KOERI (2021) The online earthquake catalog of Kandilli observatory and Earthquake Research Institute, Turkey

L'Heureux J, Long M (2017) Relationship between shear-wave velocity and geotechnical parameters for Norwegian clays. J Geotech Geoenvironm Eng 143:04017013

Lomnitz C (1999) The end of earthquake hazard. Seismol Res Lett 70:387–388. https://doi.org/10.1785/gssrl.70.4.387

Louie J (2001) Faster, better: shear-wave velocity to 100 meters depth from refraction microtremor arrays. Bull Seismol Soc Am 91:252–272

McKenzie D (1972) Active tectonics of the Mediterranean region. Geophys J Int 30:109–185

McKenzie D (1976) The East Anatolian Fault: a major structure in eastern Turkey. Earth Planet Sci Lett 29:189–193

McKenzie D (1978) Active tectonics of the Alpine- Himalayan belt: The Aegean Sea and surrounding regions (tectonic of Aegean region). Geophys J R Astron Soc 55:217–254

Mucciarelli M, Masi A, Gallipoli MR et al (2004) Evidence of soil-building resonance, building frequency shift and (maybe) site-city interaction during the 2002 Molise seismic sequence. Bull Seismol Soc Am 94:1943–1953

Muehlberger W, Gordon M (1987) Observations on the complexity of the East Anatolian Fault, Turkey. J Struct Geol 9:899–903. https://doi.org/10.1016/0191-8141(87)90091-5

Nakamura Y (1989) A method for dynamic characteristics estimation of subsurface using microtremor on the ground surface. Railw Q 30:25–53

Nakamura Y (2019) What Is the Nakamura Method? Seismol Res Lett 90:1437–1443

Nakamura Y, Saito A (1983) Estimations of seismic response char_acteristics and maximum acceleration of surface ground using strong motion records. In: 17th JSCE earthquake engineering symposium, pp 25–28

Nakamura Y (1996) Real-time information systems for hazards mitigation. In: 7th World conference on earthquake engineering, Elsevier Science, paper no. 2134

Nakamura Y (1997) Seismic vulnerability indices for ground and structures using microtremor. In: World congress on railway research in florence, Florence , Italy

Nakamura Y (2000) Clear identification of fundamental idea of Nakamura's technique and its applications. In: 12th World conference on earthquake engineering, Auckland, paper no. 2656

Nalbant S, McCloskey J, Steacy S, Barka A (2002) Stress accumulation and increased seismic risk in eastern Turkey. Earth Planet Sci Lett 195:291–298

Nogoshi M, Igarashi T (1970a) On the propagation characteristics of microtremor. Zisin 23:264–280

Nogoshi M, Igarashi T (1970b) On the amplitude characteristics of microtremor—part 1. Zisin 23:281–303

Nogoshi M, Igarashi T (1971) On the amplitude characteristics of microtremor—part 2. Zisin 24:26–40

Okada H (2006) Theory of efficient array observations of microtremors with special reference to the SPAC method. Explor Geophys 37:73–85

Okada H, Suto K (2003) The microtremor survey method. In: Society of exploration geophysicists

Pamuk E (2019) Investigation of the local site effects in the northern part of the eastern Anatolian region, Turkey. Boll Di Geofis Teore Appl 60:549–568

Pamuk E, Ozer C (2020) The site effect investigation with using horizontal-to-vertical spectral ratio method on earthquake data, South of Turkey. Geotectonics 54:563–576. https://doi.org/10.1134/S001685212004010X

Park C, Miller R, Xia J (1999) Multichannel analysis of surface waves. Geophysics 64:800–808

Park C, Miller R, Xia J, Ivanov J (2007) Multichannel analysis of surface waves (MASW)— active and passive methods. Lead Edge 26:60–64

Parolai S, Bormann P, Milkereit C (2002) New relationships between vs thickness of sediments, and resonance frequency calculated by the H/V ratio of seismic noise for the Cologne Area (Germany). Bull Seismol Soc Am 92:2521–2527. https://doi.org/10.1785/0120010248

Pavoni N (1962) Die Nordanatolische Horizontalverschiebung. Geol Rundschau 51:122–139. https://doi.org/10.1007/BF01803232

Pınar N, Lahn E (1952) Türkiye Depremleri İzahlı Kataloğu. Bayındırlık Bakanlığı, Yapı & İmar İşleri Reisliği Yayınları, Ankara

Pousse-Beltran L, Nissen E, Bergman EA et al (2020) The 2020 Mw 6.8 Elazığ (Turkey) earthquake reveals rupture behavior of the East Anatolian Fault. Geophys Res Lett. https://doi.org/10.1029/2020GL088136

Poyraz S, Aksarı D, Ergün T et al (2019) The December 2nd, 2015 Bingöl, Eastern Anatolia-Turkey, earthquake (Mw=5.3): a rupture on optimally oriented fault plane. J Asian Earth Sci 173:88–97. https://doi.org/10.1016/j.jseaes.2018.12.019

Reilinger R, McClusky S (2011) Nubia–Arabia–Eurasia plate motions and the dynamics of Mediterranean and Middle East tectonics. Geophys J Int 186:971–979

Reilinger R, McClusky S, Vernant P et al (2006) GPS constraints on continental deformation in the Africa-Arabia-Eurasia continental collision zone and implications for the dynamics of plate interactions. J Geophys Res Solid Earth 111:1–26. https://doi.org/10.1029/2005JB004051

Sançar T, Zabcı C, Akcar N et al (2020) Geodynamic importance of the strike-slip faults at the eastern part of the Anatolian Scholle: Inferences from the uplift and slip rate of the Malatya Fault (Malatya). J Asian Earth Sci 188:104091. https://doi.org/10.1016/j.jseaes.2019.104091

Sançar T, Zabcı C, Akyüz H et al (2009) Late holocene activity of Kargapazari Segment, Eastern part of the North Anatolian Fault Zone, Bingöl, Turkey. In: EGU General Assembly. Vienna, paper no. 7710

Sançar T (2016) Preliminary investigation on the deformation rates of the Nazimiye Fault (Eastern Turkey). In: EGU General Assembly 2016, Vienna, pp EGU2016-2452

Şaroğlu F, Emre Ö, Kuşçu I (1992) The East anatolian fault zone of Turkey. Ann Tectonicae 6:99–125

Şaroglu F, Yılmaz Y (1984) Doğu Anadolu'nun neotektoniği ve ilgili mağmatizması. In: T.J.K. Ketin Simpozyumu, Ankara, pp 149–162

Şaroglu F, Yılmaz Y (1986) Geological evolution and basin models during neotectonic episode in the Eastern Anatolia. Bull Miner Res Explor 107:73–94

Şaroğlu F (1985) Dogu Anadolu'nun Neotektonik Dönemde Jeolojik ve Yapısal Evrimi, İstanbul Üniversitesi

Şengör A (1979) The North Anatolian transform fault: its age, offset and tectonic significance. J Geol Soc Lond 136:269–282

Şengör A, Görür N, Şaroğlu F (1985) Strike-slip faulting and related basin formation in zones of tectonic escape: Turkey as a case study. In: Biddle K, Christie-Blick N (eds) Strike-slip deformation, basin formation and sedimentation. Society of Economic Paleontologists and Mineralogists, Tulsa, pp 227–264

Şengör A, Tüysüz O, Imren C et al (2005) The north anatolian fault: a new look. Annu Rev Earth Planet Sci 33:37–112. https://doi.org/10.1146/annurev.earth.32.101802.120415

Şengör A, Canitez N (1982) The North Anatolian Fault. In: Berkhemer H, Hsu K (eds) Alpine-mediterranean geodynamics. American Geophysical Union (AGU), pp 205–216

Şengör A (1980) Türkiye neotektoniğinin esasları. In: Türkiye Jeoloji Kurumu Konferans Serisi 2. Ankara, p 40

Seyitoğlu G, Esat K, Kaypak B, et al (2019) Internal deformation of Turkish-Iranian Plateau in the Hinterland of Bitlis-Zagros Suture Zone. In: Saein A (ed) Developments in structural geology and tectonics, vol 3, pp 161–244

Seymen İ, Aydın A (1972) The Bingöl earthquake fault and its relation to the North Anatolian Fault Zone. Bull Miner Res Explor 79:1–8

Stanko D, Markušić S (2020) An empirical relationship between resonance frequency, bedrock depth and VS30 for Croatia based on HVSR forward modelling. Nat Hazards 103:3715–3743. https://doi.org/10.1007/s11069-020-04152-z

Stanko D, Markušić S, Strelec S, Gazdek M (2017) HVSR analysis of seismic site effects and soil-structure resonance in Varaždin city (North Croatia). Soil Dyn Earthq Eng 92:666–677

Sümengen M (2011) 1/100000 Ölçekli Türkiye Jeoloji Haritaları, Elazığ K44 Paftası Raporu. Ankara, Turkey

Tan O, Tapirdamaz M, Yörük A (2008) The earthquake catalogues for Turkey. Turk J Earth Sci 17:405–418

Tan O, Pabucu Z, Taprdamaz MC et al (2011) Aftershock study and seismotectonic implications of the 8 March 2010 Kovanclar (Elazğ, Turkey) earthquake (MW = 6.1). Geophys Res Lett. https://doi.org/10.1029/2011GL047702

Tarhan N (1997) 1/100.000 Türkiye Jeoloji Haritaları Erzurum J 45 Paftası, Ankara, Turkey

Tarhan N (2007) 1/100.000 Türkiye Jeoloji Haritaları Erzincan J 44 Paftası, Ankara, Turkey

Tatar Y (1986) Elazığ çevresinde Fırat Havzasının yapısal ve jeolojik özellikleri. In: Elazığ Çevresinde Fırat Havzasının Jeolojisi ve Yeraltı Zenginlikleri Simpozyumu. Elazığ

Taymaz T et al (1991) Source parameters of large earthquakes in the East Anatolian Fault Zone (Turkey). Geophys J Int 106:537–550

Tokimatsu K, Uchida A (1990) Correlation between liquefaction resistance and shear wave velocity. Soils Found 30:33–42

Ulusay R, Aydan Ö (2005) Characteristics and geo-engineering aspects of the 2003 Bingöl (Turkey) earthquake. J Geodyn 40:334–346. https://doi.org/10.1016/j.jog.2005.07.018

USGS—United States Geological Survey/Earthquake Hazards Programme/Earthquake Catalog. https://earthquake.usgs.gov/

Utkucu M, Budakoğlu E, Çabuk M (2018) Teleseismic finite-fault inversion of two M w = 6.4 earthquakes along the East Anatolian Fault Zone in Turkey: the 1998 Adana and 2003 Bingöl earthquakes. Arab J Geosci 11:1–14. https://doi.org/10.1007/s12517-018-4089-y

Vucetic M (1992) Soil properties and seismic response. In: Proceedings of the 10th world conference on earthquake engineering, pp 19–24

Westaway R (1994) Present-day kinematics of the Middle East and eastern Mediterranean. J Geophys Res 99:12071–12090. https://doi.org/10.1029/94jb00335

Westaway R, Arger J (1996) The Gölbaşı basin, southeastern Turkey: a complex discontinuity in a major strike-slip fault zone. Geol Soc Lond Spec Publ 153:729–743

Yalçınkaya E (2010) Zemin neden bu kadar önemli? Jeofizik Bülteni 63:77–80

Yavasoglu H (2015) Strain rate analysis on the Çankırı-Bingöl segment of the North Anatolian Fault in Turkey. Earth Sci Res J 19:121–127

Yılmaz O (1975) Casas Bölgesi (Bitlis Masifi) kayaçlarının petrografik ve stratigrafik incelenmesi. Türkiye Jeol Bülteni 18:33–40

Yılmaz Y, Şaroglu F, Güner Y (1987) Initation of the Neomagmatism in East Anatolia. Tectonophysics 134:177–199. https://doi.org/10.1016/0040-1951(87)90256-3

Yılmaz Y (1978) Gevaş (Van) dolayında Bitlis Masifi / ofiyolit ilişkisi. In: Türkiye 4. Petrol Kongresi, Ankara, pp 83–93

Yönlü Ö, Altunel E, Karabacak V (2017) Geological and geomorphological evidence for the southwestern extension of the East Anatolian Fault Zone, Turkey. Earth Planet Sci Lett 469:1–14

Youn J, Choo Y, Kim D (2008) Measurement of small-strain shear modulus G max of dry and saturated sands by bender element, resonant column, and torsional shear tests. Can Geotech J 45:1426–1438

Zabcı C, Akyüz HS, Sançar T (2017) Palaeoseismic history of the eastern part of the North Anatolian Fault (Erzincan, Turkey): implications for the seismicity of the Yedisu seismic gap. J Seismol 21:1407–1425. https://doi.org/10.1007/s10950-017-9673-1